Percolation in spatial evolutionary prisoner's dilemma game on two-dimensional lattices

Woosik Choi, Soon-Hyung Yook, and Yup Kim*

Department of Physics and Research Institute for Basic Sciences, Kyung Hee University, Seoul 130-701, Korea

(Received 17 August 2015; revised manuscript received 5 November 2015; published 30 November 2015)

We study the spatial evolutionary prisoner's dilemma game with updates of imitation max on triangular, hexagonal, and square lattices. We use the weak prisoner's dilemma game with a single parameter b. Due to the competition between the temptation value b and the coordination number z of the base lattice, a greater variety of percolation properties is expected to occur on the lattice with the larger z. From the numerical analysis, we find six different regimes on the triangular lattice ($z = 6$). Regardless of the initial densities of cooperators and defectors, cooperators always percolate in the steady state in two regimes for small b. In these two regimes, defectors do not percolate. In two regimes for the intermediate value of b, both cooperators and defectors undergo percolation transitions. The defector always percolates in two regimes for large b. On the hexagonal lattice ($z = 3$), there exist two distinctive regimes. For small b, both the cooperators and the defectors undergo percolation transitions while only defectors always percolate for large b. On the square lattice ($z = 4$), there exist three regimes. Combining with the finite-size scaling analyses, we show that all the observed percolation transitions belong to the universality class of the random percolation. We also show how the detailed growth mechanism of cooperator and defector clusters decides each regime.

DOI: 10.1103/PhysRevE.92.052140 PACS number(s): 02.50.Le, 05.70.Fh, 64.60.ah

I. INTRODUCTION

To understand the origin of the emergence and persistence of cooperation among selfish individuals, game theories have been studied extensively over the past few decades [1,2]. Recently, many studies have focused on spatial evolutionary games to understand how steady-state strategies emerge in various structures and to identify the characteristic features of steady-state strategies [2–4].

Among spatial evolutionary games, the *spatial evolutionary prisoner's dilemma game* (*SEPDG*) has attracted considerable attention [3,5–21]. In this paper, we consider SEPDG on two-dimensional lattices, which is defined as follows. Initially, *cooperators* (Cs) and *defectors* (Ds) are randomly distributed to sites on a lattice. The number $N_C(t)$ of C sites and $N_D(t)$ of D sites vary over time t under the condition $N_C(t) + N_D(t) = N$, where N is the total number of sites. In each update, a site is randomly selected. Then, the accumulated payoffs of the selected site and z nearest neighbors (NNs) of the site are calculated.

In the prisoner's dilemma game, if both players cooperate, then both get the payoff R (reward). If one cooperates while the other defects, D gets T (temptation) while C gets S (sucker's payoff). If both defect, they each get P (punishment). T, R, P, and S should obey the conditions $T > R > P > S$ and $2R > T + S$. Various versions of the prisoner's dilemma game have been suggested and studied, including a game with two parameters or with $(R,T,S,P) = (1,1 + D_g, -D_r,0)$ [5–7]. The prisoner's dilemma game with a single parameter such as $D_g = D_r = r$ has also been considered [7,8]. In this paper, the weak prisoner's dilemma game with $R = 1$, $T = b(1 < b < 2)$, and $P = S = 0$, which was first suggested in Ref. [9], is used. Therefore, in our SEPDG the accumulated payoff of a D site is bn_C and that of a C site is n_C, where n_C (n_D) is the number of C (D) NNs of a given site with $n_C + n_D = z$.

Some models for SEPDG [3,7,10–14] have used stochastic updates in which the strategy of the selected site is changed by some probability based on a comparison between payoffs. In this paper, we take the updates of imitation max [6–8,13,14] in which the selected site takes the strategy of the site that has the highest accumulated payoff among those of the selected site and z NNs. The results of SEPDG with the stochastic updates could be different from those with the updates of imitation max.

It has been known that the formation of *cooperator clusters* (*C clusters*) plays an important role in promoting cooperation in SEPDGs [10–12]. Therefore, it is very important to study connectivity or percolation properties of Cs and Ds as well as densities to understand the emergence of cooperation among selfish individuals. For the connectivity, some of the previous studies have shown that the final density of Cs depends on the initial density [7,8] and spatial structures [8,11,12]. Previous investigations have also focused on the structural properties and pattern formations of C clusters [9–12,15]. In particular, special patterns of C clusters and D clusters, such as evolutionary kaleidoscopes, have been found in SEPDG with synchronized updates [9,15] as a kind of cellular automata [22]. Furthermore, network reciprocity, which can be decomposed into two periods (END and EXP, as long as one starting archetype is the initial cooperation density), has been found [7,8,13,14]. The reciprocity may elucidate what determines the final cooperation density among initial cooperation density, domain size, or others.

The theory of percolation describing large-scale connectivity on lattices has now been well established to a deeper level [23]. Therefore, if cluster formation is important, the percolation properties of clusters must be studied quantitatively from the perspective of modern percolation theory. Several percolation-related studies of SEPDG with stochastic updates have been done. In Refs. [16,17], it was shown that a population density close to the percolation threshold is optimal for the successful evolution of cooperation. Another study [18] investigated some percolation properties of an

*ykim@khu.ac.kr

off-lattice SEPDG. On the other hand, the percolation properties in SEPDG with updates of imitation max have hardly been studied except for Ref. [19]. In Ref. [19], the following percolation properties of steady-state C clusters in SEPDG with updates of imitation max on a square lattice were obtained only by numerical simulations without any theoretical explanation: For $1 < b < 4/3$, C clusters were shown to undergo the percolation transition with the universality class of random (ordinary) percolation. For $4/3 < b < 3/2$, C clusters were shown to be finite regardless of the initial density of Cs. For $3/2 < b < 2$, C clusters were argued to undergo the percolation transition with the universality class of invasion percolation with trapping [24] via a comparison between critical exponents β/ν and γ/ν of the transition and the calculated β/ν from the fractal dimension d_f of the cluster [24] of the invasion percolation by a brute force application of the formula $d_f = d - \beta/\nu$ [23] without any theoretical background. Furthermore, invasion percolation does not have the phase transition, and thus the critical exponents β, ν, and γ cannot be defined. Physically, one should be careful to establish the universality class numerically when there is no theoretical or analytical basis. However, Ref. [19] paid little attention to such theoretical grounds for numerical results.

In this sense, we study the percolation properties of both Cs and Ds in SEPDG with the updates of imitation max by using *finite-size scaling* (*FSS*) analyses [23] from the following theoretical perspectives. Cs should form compact clusters for survival. For growth or expansion, Cs should have a sufficient number of C NNs. In contrast, Ds should have enough C NNs or penetrate into C clusters for survival and growth. These theoretical perspectives are supported by the well-known mean-field behavior in which increasing z brings about the extinction of Cs [2,3]. Furthermore, it has been shown that the topological properties of the lattice affect the spreading and maintenance of cooperation [20,21]. Hence, the percolation properties should be decided by the competition between b and the coordination number z of the base lattice.

To illustrate the validity of this perspective or to confirm that on the lattice with larger z there is a greater variety of regimes (cluster structures) in the steady state, we study the connectivity or the percolation properties of SEPDG with the updates of imitation max on triangular, hexagonal (honeycomb), and square lattices. Our analyses focus not only on the percolation properties of the steady-state clusters but also on theoretical explanations of the properties through growing mechanism of clusters. Due to the interdependence of Cs and Ds in SEPDG, we focus on the connectivity or the percolation property of *defector clusters* (*D clusters*) as well as C clusters in the steady state.

We find the following important results. On the triangular lattice ($z = 6$), there exist six regimes: two C-dominant regimes for low b, two regimes of percolation transitions for mid b, and two D-dominant regimes for high b. On the hexagonal lattice ($z = 3$), there exist only two regimes, namely a regime of percolation transition for low b and a D-dominant regime for high b. As in Ref. [19], we find three regimes on the square lattice. Furthermore, the universality of any percolation transition on any lattice is clearly shown to belong to that of the random percolation.

II. PERCOLATION PROPERTIES

We performed a simulation to investigate the property of C clusters and D clusters [23] in the steady state depending on the parameter b. The steady state in a given simulation run means the state in which $N_{C(D)}(t)$ hardly varies against t. As we shall see, most steady states are absorbing states in which the spatial distribution of strategies is frozen or quenched [3]. We also find that a local strategy reversal process occurs in several steady states for $3/2 < b < 5/3$ (the fifth regime) and $5/3 < b < 2$ (the sixth regime) on the triangular lattice, for $4/3 < b < 3/2$ (the second regime) on the square lattice, and for $3/2 < b < 2$ (the second regime) on the hexagonal lattice. However, this reversal process rarely affects the macroscopic properties.

To study the percolation transition of C and D clusters, we first measure the final densities, $p_f^{C(D)}$, the fractions of the largest clusters, $P_{LC}^{C(D)}$, and the susceptibility, $\chi^{C(D)}$, against the initial densities $p_i^{C(D)}$. These quantities are defined as follows [23,25]:

$$p_i^C = \frac{N_C(t=0)}{N}, \quad p_i^D = \frac{N_D(t=0)}{N}, \tag{1}$$

$$p_f^C = \frac{\langle N_C(t\to\infty)\rangle}{N}, \quad p_f^D = \frac{\langle N_D(t\to\infty)\rangle}{N}, \tag{2}$$

$$P_{LC}^C = \frac{\langle N_{LC}^C\rangle}{N}, \quad P_{LC}^D = \frac{\langle N_{LC}^D\rangle}{N}, \tag{3}$$

$$\chi^C = N\left[\langle P_{LC}^{C2}\rangle - \langle P_{LC}^C\rangle^2\right], \quad \chi^D = N\left[\langle P_{LC}^{D2}\rangle - \langle P_{LC}^D\rangle^2\right], \tag{4}$$

where $N_{LC}^{C(D)}$ is the number of sites of the largest C (D) cluster, and $\langle\cdots\rangle$ stands for the average over steady-state configurations. All quantities are obtained by averaging over more than 10^4 simulation runs. Since our model uses the updates of imitation max, the percolation properties should be identical in a given interval of b for a specific regime on any lattice.

A. Strategy decision

Before presenting the simulation results, we want to explain the theoretical basis for how the different regimes for connectivity or percolation properties occur on different lattices. The theoretical basis is the strategy decision process in a typical update of imitation max. In each update, the strategy of the selected site is decided by the highest accumulated payoff among those of the $z + 1$ sites, i.e., the selected site and its z NNs. Thus, the strategy of the site is decided by the comparison between the highest payoff P_h^C of C sites and the highest payoff P_h^D of D sites among the $z + 1$ sites. The selected site will take C if $P_h^C > P_h^D$. Otherwise, the site will take D. Possible values of P_h^C and P_h^D depend on z. On the hexagonal lattice with $z = 3$, the set of possible values of P_h^C (P_h^C set) is $\{0,1,2,3\}$ and that of P_h^D (P_h^D set) is $\{0,b,2b,3b\}$. When $P_h^D = 0$, any site that is involved in calculating the payoffs of the $z + 1$ sites cannot be a C site on the hexagonal lattice. Thus, we do not have to compare $P_h^D = 0$ to any element in P_h^C. The other 12 comparisons shown in Fig. 1(a) can occur at the selected sites of the hexagonal lattice. Except for the comparison between $P_h^C = 3$ and $P_h^D = 2b$, the

(a)

P_h^D \ P_h^C	0	1	2	3
0				
b	D	D	C	C
$2b$	D	D	D	C if $b<3/2$ D if $b>3/2$
$3b$	D	D	D	D

(b)

P_h^D \ P_h^C	0	1	2	3	4
0					
b	D	D	C	C	C
$2b$	D	D	D	C if $b<3/2$ D if $b>3/2$	C
$3b$	D	D	D	D	C if $b<4/3$ D if $b>4/3$
$4b$	D	D	D	D	D

(c)

P_h^D \ P_h^C	0	1	2	3	4	5	6
0							
b	D	D					
$2b$	D	D	D	C if $b<3/2$ D if $b>3/2$	C	C	C
$3b$	D	D	D	D	C if $b<4/3$ D if $b>4/3$	C if $b<5/3$ D if $b>5/3$	C
$4b$	D	D	D	D	D	C if $b<5/4$ D if $b>5/4$	C if $b<3/2$ D if $b>3/2$
$5b$		D	D	D	D	D	C if $b<6/5$ D if $b>6/5$
$6b$			D	D	D	D	D

FIG. 1. The strategy-decision tables for the comparisons between P_h^C and P_h^D (a) on the hexagonal lattice ($z = 3$) (in Fig. 14), (b) on the square lattice ($z = 4$) (in Fig. 15), and (c) on the triangular lattice ($z = 6$) (in Fig. 3). The comparisons denoted by "X" cannot occur at the selected sites on the corresponding lattice. The strategy decisions for the most comparisons do not depend on b. The strategy decisions for some special comparisons depend on b. For example, for the comparison between $P_h^C = 3$ and $P_h^D = 2b$ on the hexagonal lattice, the strategy is decided as C if $b < 3/2$ or as D if $b > 3/2$.

strategies are simply decided for the remaining 11 comparisons regardless of b, as shown in Fig. 1(a). For the comparison between $P_h^C = 3$ and $P_h^D = 2b$, the strategy is decided as C if $b < 3/2$ or as D if $b > 3/2$. Therefore, there can arise two regimes for the percolation properties on the hexagonal lattice, one in the interval $1 < b < 3/2$ and the other in $3/2 < b < 2$. On the square lattice, the P_h^C set is $\{0,1,2,3,4\}$ and the P_h^D set is $\{0,b,2b,3b,4b\}$. As on the hexagonal lattice, the strategy-decision table for the possible 20 comparisons on the square lattice is displayed in Fig. 1(b). Thus, there can arise three regimes on the square lattice, one in $1 < b < 4/3$, another in $4/3 < b < 3/2$, and the third in $3/2 < b < 2$. On the triangular lattice, the P_h^C set is $\{0,1,2,3,4,5,6\}$ and the P_h^D set is $\{0,b,2b,3b,4b,5b,6b\}$. Among the 49 comparisons between the two sets, the comparisons of $P_h^D = 0$ do not have to be considered as on hexagonal and square lattices. Moreover, the eight comparisons, $(P_h^C, P_h^D) = (0,5b)$, $(0,6b)$, $(1,6b)$, $(2,b)$, $(3,b)$, $(4,b)$, $(5,b)$, and $(6,b)$, do not occur for any selected site on the triangular lattice. The strategy-decision table for the possible 34 comparisons on the triangular lattice is displayed in Fig. 1(c). Thus, there can arise six regimes, one in $1 < b < 6/5$, another in $6/5 < b < 5/4$, another in $5/4 < b < 4/3$, another in $4/3 < b < 3/2$, another in $3/2 < b < 5/3$, and the last in $5/3 < b < 2$. From the strategy-decision tables in Fig. 1, we can easily understand the mechanism for why different regimes occur depending on b. We now study the percolation property for a specific regime on the corresponding lattice via a simulation.

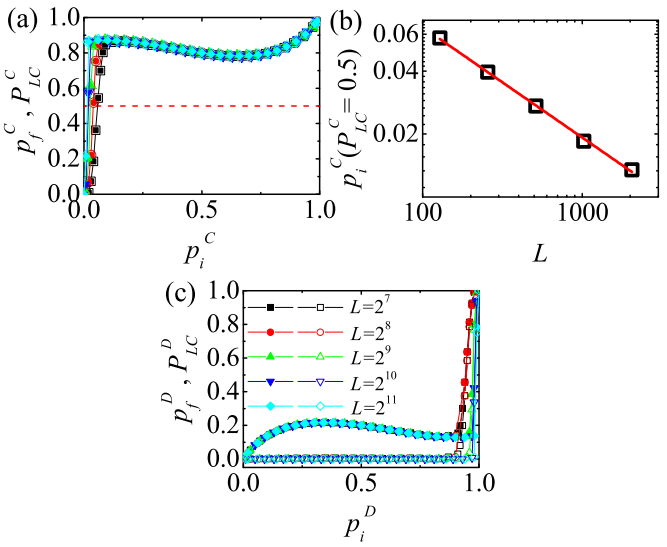

FIG. 2. (Color online) Plots of the first regime or for $1 < b < 6/5$ on the triangular lattice. (a) Plots of $p_f^C(p_i^C, L)$ and $P_{LC}^C(p_i^C, L)$ against p_i^C. (b) Plot of $p_i^C(P_{LC}^C = 0.5)$ against L. The straight line represents the relation $p_i^C(P_{LC}^C = 0.5) = 0.77 \times L^{-0.54}$. (c) Plots of $p_f^D(p_i^D, L)$ and $P_{LC}^D(p_i^D, L)$ against p_i^D. Filled symbols stand for p_f's and open symbols stand for P_{LC}'s in any plot in this paper.

B. Triangular lattice

We first investigate the connectivity or the percolation properties of C clusters and D clusters on the triangular lattice.

The first regime occurs for $1 < b < 6/5$, as shown in Fig. 2. $p_f^C(p_i^C, L)$, $P_{LC}^C(p_i^C, L)$, $p_f^D(p_i^D, L)$, and $P_{LC}^D(p_i^D, L)$ are measured using lattice sizes $L = 2^7 - 2^{11}$. We find that $P_{LC}^C(p_i^C, L) \simeq p_f^C(p_i^C, L) > 0.78$ except for very small p_i^C [Fig. 2(a)]. Hence, the infinite C cluster always exists in the steady state, and nearly all C sites are in the infinite C cluster except for very small p_i^C. We study the dependence of $p_i^C(P_{LC}^C = 0.5, L)$ on L to find $p_i^C(P_{LC}^C = 0.5, L) \sim L^{-0.54(1)}$ as in Fig. 2(b), confirming that the behaviors for very small p_i^C disappear in the limit $L \to \infty$. In contrast, $P_{LC}^D(p_i^D, L) \simeq 0$ although $p_f^D(p_i^D, L) > 0$ [Fig. 2(c)]. Thus, in the first regime, C sites always percolate and D sites form only finite isolated clusters for all $p_i^C(p_i^D)$.

The first regime originates from the growth process in which a special finite C cluster is stable against any update in our model and grows indefinitely by a certain series of updates. As shown in Fig. 3(a), the special C cluster is the diamond-type C cluster. If there is no diamond-type C cluster, it is confirmed that initial isolated C clusters disappear by updating processes and D sites cover the entire lattice in the steady state. On the other hand, if at least one diamond-type C cluster exists initially, the C cluster grows into an infinite cluster and only finite D clusters remain in the steady state. The isolated diamond-type C cluster is stable against any update in our model for $1 < b < 6/5$, because the highest payoff of C sites in the cluster is 3 and that of the surrounding D sites is $2b(< 3)$ [Fig. 3(a)]. Furthermore, if the selected site in an update is a ① D site of Fig. 3(a), the site changes into the C site because of $2b < 3$. The repetition of the growth process makes a larger C cluster in which the diamond-type C clusters overlap and

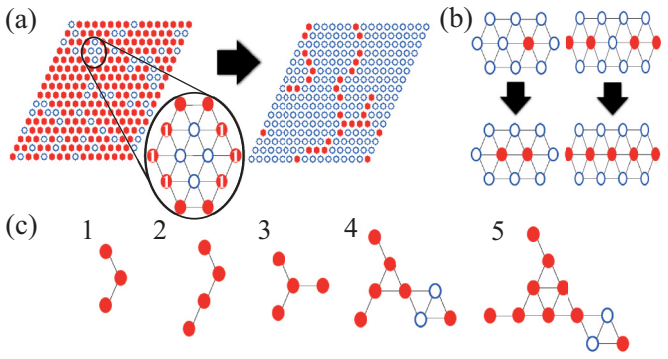

FIG. 3. (Color online) (a) Evolution of an initial configuration containing a diamond-type C cluster ($\diamond$) to the steady-state configuration, in which C sites form an infinite cluster and only finite isolated D clusters remain. (b) Two growth processes of D clusters. There exist no growth processes of D clusters except the two growth processes. (c) Some of the stable base patterns of D clusters. Blue (open) circles and red (filled) circles represent Cs and Ds in any figure of configurations, respectively.

connect to one another. The base diamond-type C cluster must exist for any $p_i^C (\neq 0)$ in the limit $L \to \infty$ because the initial average number of clusters is equal to $L^2 p_i^{C4}(1-p_i^C)^{10}$ [23]. Therefore, in the first regime for $1 < b < 6/5$, for any $p_i^C (\neq 0)$ there exists only one stable C cluster that always percolates.

P_{LC}^C decreases slightly from 0.83 to 0.78 as p_i^C increases from 0 to 0.7, whereas P_{LC}^C increases for $p_i^C > 0.7$ [Fig. 2(a)]. To understand this unexpected behavior, stable base patterns of D clusters are studied. Some of these stable base patterns are illustrated in Figs. 3(b) and 3(c). As shown in Fig. 3(b), an isolated D site grows into the two-site D cluster, and two line-type D clusters grow into a line-type cluster of 5 Ds. Except for these growths, no D cluster can grow, rather it shrinks into a stable cluster. We also confirm that the steady state consisting of the percolating C cluster and the stable D clusters is an absorbing state [3]. For small p_i^D, D sites are isolated. Since an isolated D site grows into the two-site D cluster, p_f^D increases as p_i^D increases from 0. In contrast, for large p_i^D, the initial large D clusters must shrink into one of the stable D clusters. Thus, p_f^D decreases as p_i^D increases in the large p_i^D region. These growth mechanisms explain how P_{LC}^C (p_f^D) increases for $p_i^C > 0.7$ ($p_i^D < 0.3$) and P_{LC}^C (p_f^D) decreases for $p_i^C < 0.7$ ($p_i^D > 0.3$).

In the second regime for $6/5 < b < 5/4$, we find $p_f^C \simeq 0.7$ regardless of p_i^C and L except for very small p_i^C, as shown in Fig. 4(a). The finite-size effect for very small p_i^C is the same as that in the first regime. P_{LC}^C also does not depend on p_i^C but decreases as L increases. $P_{LC}^C(L \to \infty) = 0.50(1)$ is obtained by the fitting $P_{LC}^C(L) = P_{LC}^C(L \to \infty) + 4.7(7) \times L^{-1.00(1)}$ as in Fig. 4(b). Hence, there exists an infinite C cluster for all p_i^C in the steady state. $p_f^D \simeq 0.3$ for any $p_i^D(p_i^C)$, whereas P_{LC}^D decreases as L increases as $P_{LC}^D \sim \exp(-aL)$ [Figs. 4(c) and 4(d)]. Therefore, in the second regime, a C cluster in the steady state always percolates and D clusters form only finite clusters as in the first regime.

The growth mechanism of a C cluster in the second regime is nearly the same as that in the first regime. But, in contrast

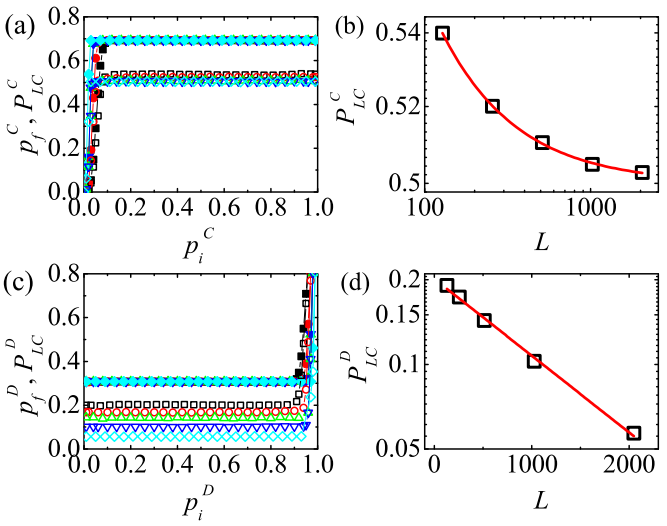

FIG. 4. (Color online) Plots of the second regime or for $6/5 < b < 5/4$. (a) Plots of $p_f^C(p_i^C, L)$ and $P_{LC}^C(p_i^C, L)$ against p_i^C. (b) Plot of P_{LC}^C against L. The red curve represents the relation $P_{LC}^C(L) = P_{LC}^C(\infty) + 4.7 \times L^{-1}$, with $P_{LC}^C(\infty) = 0.50$. (c) Plots of $p_f^D(p_i^D, L)$ and $P_{LC}^D(p_i^D, L)$ against p_i^D. (d) Plot of P_{LC}^D against L. The straight line represents the relation $P_{LC}^D = 0.20 \times \exp(-0.0006L)$. Symbols stand for the same quantity as those in Fig. 2.

to the first regime, the growth from a single diamond-type C cluster produces not only an infinite cluster but finite clusters because of the different growth mechanism of D clusters. Stable D clusters in the second regime are also combinations of the base patterns in Figs. 3(b) and 3(c). However, the growth mechanism of D clusters in the second regime is different from that in the first regime. The accumulated payoff of the free end of the line part of a D cluster is $5b$, which is larger than the highest accumulated payoff of a C site or 6. Thus, such a free end D site can grow. The growth of a D cluster stops if any D cluster forms a certain combination of stable patterns without the free end D sites, as in Fig. 5. Therefore, any initial state in

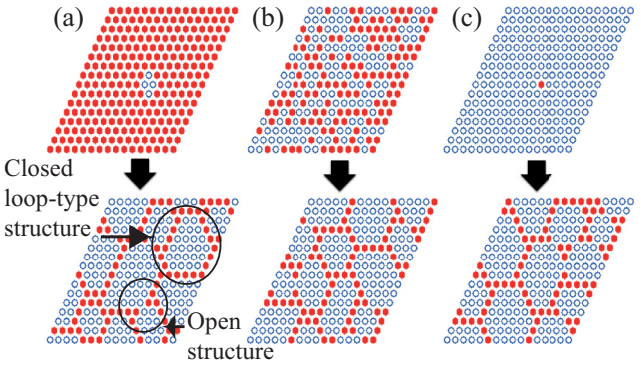

FIG. 5. (Color online) (a) Steady-state configuration (SSC) from the initial configurations with a single diamond-type C cluster. (b) SSC from the initial configuration with $p_i^C = 0.5$. (c) SSC from an isolated D site. Any of the SSCs has two main configurations of D clusters. One is the closed loop-type structure, and the other is the open structure between stable ends.

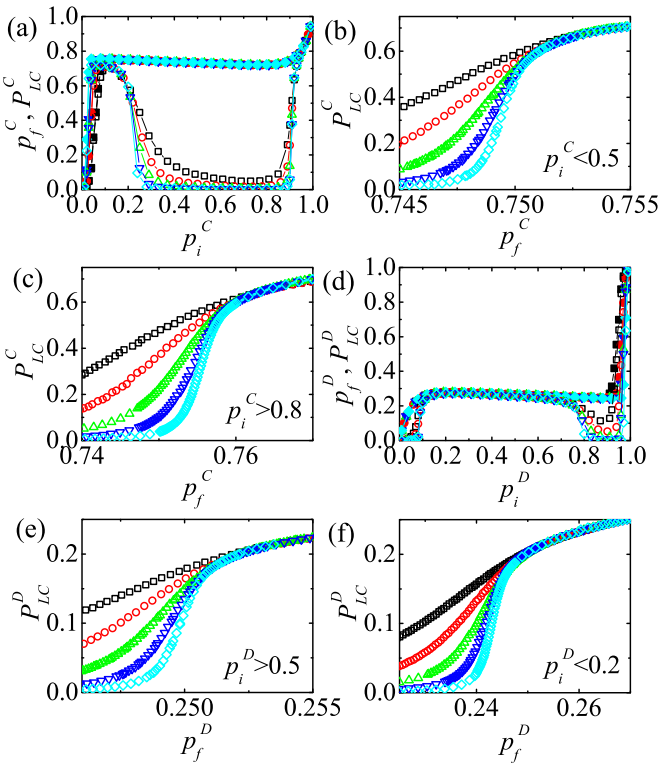

FIG. 6. (Color online) Plots of the third regime or for $5/4 < b < 4/3$. (a) Plots of $p_f^C(p_i^C,L)$ and $P_{LC}^C(p_i^C,L)$ against p_i^C. (b) Plot of $P_{LC}^C(p_f^C,L)$ against p_f^C for $p_i^C < 0.5$. (c) Plot of $P_{LC}^C(p_f^C,L)$ against p_f^C for $p_i^C > 0.8$. (d) Plots of $p_f^D(p_i^D,L)$ and $P_{LC}^D(p_i^D,L)$ against p_i^D. (e) Plot of $P_{LC}^D(p_f^D,L)$ against p_f^D for $p_i^D > 0.5$. (f) Plot of $P_{LC}^D(p_f^D,L)$ against p_f^D for $p_i^D < 0.2$.

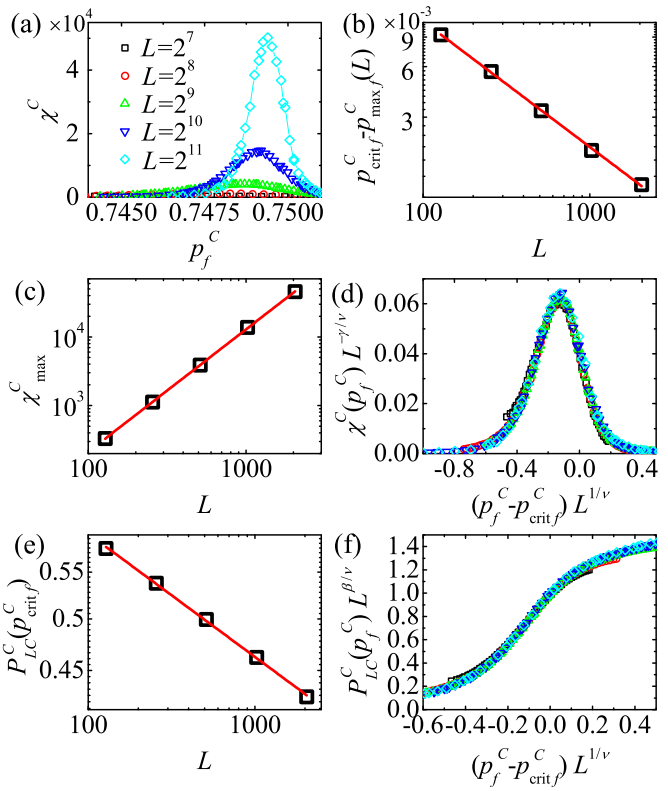

FIG. 7. (Color online) Finite-size scaling analyses for $p_i^C < 0.5$ in the third regime. (a) Plot of $\chi^C(p_f^C,L)$ against p_f^C. (b) Plot of $[p_{\mathrm{crit}f}^C - p_{\max f}^C(L)] \sim L^{-1/\nu}$ with $p_{\mathrm{crit}f}^C = 0.7498(1)$ and $1/\nu = 0.75(1)$. (c) Plot of $\chi_{\max}^C \sim L^{\gamma/\nu}$ with $\gamma/\nu = 1.78(1)$. (d) The scaling plot of $\chi^C(p_f^C,L)L^{-\gamma/\nu}$ against $(p_f^C - p_{\mathrm{crit}f}^C)L^{1/\nu}$ with $p_{\mathrm{crit}f}^C = 0.7498$, $\gamma/\nu = 1.78$, and $1/\nu = 0.75$. (e) Plot of $P_{LC}^C(p_{\mathrm{crit}f}^C) \sim L^{-\beta/\nu}$ with $\beta/\nu = 0.11(1)$. (f) The scaling plot of $P_{LC}^C(p_f^C,L)L^{\beta/\nu}$ against $(p_f^C - p_{\mathrm{crit}f}^C)L^{1/\nu}$ with $\beta/\nu = 0.11$.

the second regime evolves into a self-organized steady state, as shown in Fig. 5.

The average over these self-organized states gives $p_f^C \simeq 0.7$ and $p_f^D \simeq 0.3$ regardless of p_i^C (p_i^D) and L. D clusters in the self-organized states have two main substructures. One is the closed-loop-type structure, and the other is the open structure between stable ends, as shown in Fig. 5(a). Because any D cluster consists of only two main substructures, any self-organized steady state is an absorbing state [3]. P_{LC}^C is smaller than p_f^C because of the closed-loop-type structures. In contrast, the open structures hinder the formation of large D clusters and assist the growth of larger C clusters. For small L, the closed-loop-type structures make $P_{LC}^D > 0$. As L increases, the number N_s of the open structures increases and P_{LC}^D decreases, as in Figs. 4(c) and 4(d). In the limit $L \to \infty$, there cannot exist an infinite D cluster or $P_{LC}^D \to 0$ because $N_s \to \infty$. P_{LC}^C also decreases with L because of the closed loop-type D clusters. However, $P_{LC}^C(L \to \infty) > 0$ because of D clusters with open structures.

The third regime occurs for $5/4 < b < 4/3$, as shown in Fig. 6. p_f^C decreases from 0.76 to 0.72 as p_i^C increases to 0.8 but it increases to 1 for $p_i^C > 0.8$ [Fig. 6(a)]. In contrast, P_{LC}^C exhibits very complicated behavior. For small p_i^C, P_{LC}^C decreases. Then, P_{LC}^C seems to approach 0 for moderate p_i^C and rapidly increases for $p_i^C > 0.9$. The dependences of P_{LC}^C on p_f^C for both $p_i^C < 0.5$ and $p_i^C > 0.8$ are shown in Figs. 6(b) and 6(c). Interestingly, the percolation transition of C clusters with increasing p_f^C is clearly observed. In particular, the transition for $p_i^C < 0.5$ is nearly identical to that for $p_i^C > 0.8$. The meaning of the result in Figs. 6(b) and 6(c) is that percolating phases with the infinite C cluster exist for large p_f^C, which occurs not only for large p_i^C(>0.95) but also for small p_i^C(<0.15). For moderate p_i^C, there exist only finite C clusters.

To analyze the percolation transition for $p_i^C < 0.5$, $\chi^C(p_f^C,L)$ in Eq. (4) is first studied [Fig. 7(a)]. From the finite-size-scaling (FSS) relation $[p_{\mathrm{crit}f}^C - p_{\max f}^C(L)] \sim L^{-1/\nu}$ [23], we obtain $1/\nu = 0.75(1)$ and $p_{\mathrm{crit}f}^C = 0.7498(1)$ for $p_i^C < 0.5$ as in Fig. 7(b). Here, $p_{\max f}^C$ is the p_f^C at which $\chi^C(p_f^C,L)$ is maximal and $p_{\mathrm{crit}f}^C$ is the critical density at which the percolation transition on the infinite-sized lattice occurs [23]. From the FSS ansatz for the maximal value of $\chi^C(p_f^C,L)$, $\chi_{\max}^C \sim L^{\gamma/\nu}$ [23], $\gamma/\nu = 1.78(1)$ is also obtained as in Fig. 7(c). $\chi^C(p_f^C,L)$ satisfies the FSS relation [23]

$$\chi^C\left(p_f^C,L\right) = L^{\gamma/\nu} f\left[\left(p_f^C - p_{\mathrm{crit}f}^C\right)L^{1/\nu}\right], \qquad (5)$$

with $1/\nu = 0.75$, $p_{\mathrm{crit}f}^C = 0.7498$, and $\gamma/\nu = 1.78$ as shown in Fig. 7(d). From $P_{LC}^C(p_{\mathrm{crit}f}^C) \sim L^{-\beta/\nu}$ [23] and $p_{\mathrm{crit}f}^C = 0.7498$,

we also obtain $\beta/\nu = 0.11(1)$ [Fig. 7(e)]. Thus, P^C_{LC} also satisfies FSS [23],

$$P^C_{LC}(p^C_f, L) = L^{-\beta/\nu} g\left[\left(p^C_f - p^C_{\mathrm{crit}f}\right) L^{1/\nu}\right], \qquad (6)$$

with $\beta/\nu = 0.11$, $1/\nu = 0.75$, and $p^C_{\mathrm{crit}f} = 0.7498$ as in Fig. 7(f). We also investigate the transition property of C clusters for $p^C_i > 0.8$ in the same way as for $p^C_i < 0.5$, and we obtain $p^C_{\mathrm{crit}f} = 0.7564(1)$ and the same critical exponents. The measured critical exponents of both transitions for $p^C_i < 0.5$ and for $p^C_i > 0.8$ are nearly identical to the exact values of exponents, $\nu = 4/3$, $\beta/\nu = 5/48$, and $\gamma/\nu = 43/24$ of the random percolation in two dimensions [23]. This result means that the universality of the critical phenomena for both percolation transitions of C clusters belongs to that of the random percolation.

In Figs. 6(d)–6(f), we also investigate the properties of D clusters in the third regime in the same way as for C clusters. P^D_{LC} also shows very complicated behavior. For small p^D_i, P^D_{LC} rapidly increases. Then, $P^D_{LC} \simeq p^D_f > 0$ for moderate p^D_i and P^D_{LC} rapidly decreases for $p^D_i > 0.7$ [Fig. 6(d)]. As shown in Figs. 6(e) and 6(f), the percolation phase transition of the D cluster depending on p^D_f is also clearly observed. The D-cluster transition for $p^D_i < 0.2$ ($p^C_i > 0.8$) is also nearly identical to that for $p^D_i > 0.5$ ($p^C_i < 0.5$). From the same FSS analyses of the D-cluster transitions for $p^D_i < 0.2$ and $p^D_i > 0.5$, we obtain $p^D_{\mathrm{crit}f} = 0.2436(1)$ for $p^D_i < 0.2$ and $p^D_{\mathrm{crit}f} = 0.2502(1)$ for $p^D_i > 0.5$ as well as the same critical exponents as those for the C-cluster transitions. These results imply that both C clusters and D clusters in the third regime undergo nearly identical percolation transitions if the control parameter is p^C_f (p^D_f). In terms of p^C_i (p^D_i), there exist two percolation transitions, one for small p^C_i (or large p^D_i) and the other for large p^C_i (or small p^D_i).

The growth of a single diamond-type seed C cluster in the third regime produces not only an infinite C cluster but finite clusters. As in the second regime, any free end of the line-type part of a D cluster can grow in the third regime. More new patterns of D clusters in Fig. 8(a) as well as those in Fig. 3(c) become stable in the third regime. In this regime, as in the first regime, we find that any steady state is an absorbing state [3]. Therefore, in the third regime, there can be many more chances to form the stable D clusters than in the second regime. Thus, for small p^D_i, the number of stable isolated D clusters increases as p^D_i increases. As p^D_i increases, these isolated D clusters merge with one another to form a large cluster, as shown in Fig. 8(b). This process explains the percolation transition for $p^D_i < 0.2$ ($p^C_i > 0.8$). In contrast, the transition for $p^D_i > 0.5$ ($p^C_i < 0.5$) in the third regime is rather anomalous. To understand this anomalous transition, the dependences of p^C_f and P^C_{LC} on the initial density n_d of the diamond-type seed C clusters are investigated as in Fig. 8(c). The growing C cluster from a single diamond-type C cluster produces an infinite cluster with $P^C_{LC} \simeq 0.70$ and $p^C_f \simeq 0.76$, which are nearly identical to P^C_{LC} and p^C_f for very small p^C_i in Fig. 6. As n_d increases, p^C_f decreases slowly, but P^C_{LC} sharply decreases to 0 around $n_d \simeq 0.003$. For the quantitative analyses, $n_d(P^C_{LC} = 0.1)$ is evaluated to find $n_d(P^C_{LC} = 0.1, L) = n_d(\infty) + 1.8(1) \times L^{-1.15(1)}$, where

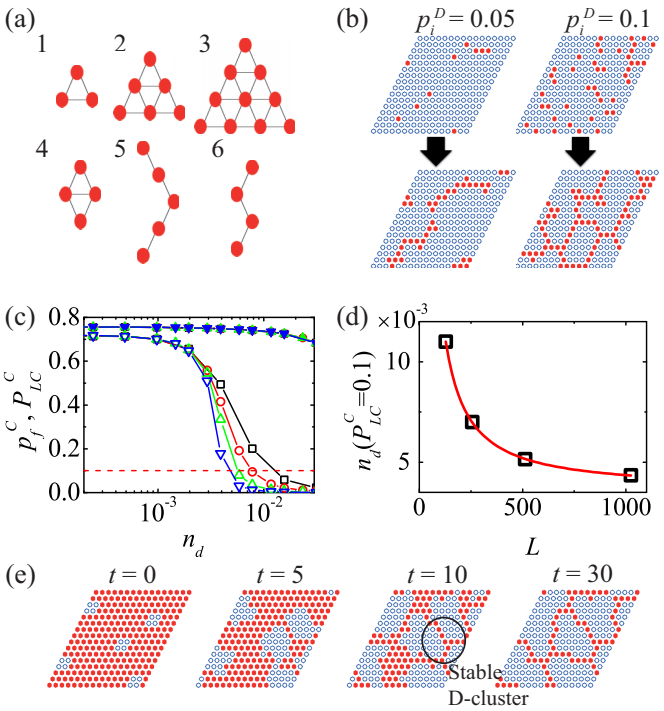

FIG. 8. (Color online) (a) New stable base patterns of D clusters in the third regime. (b) Steady-state configurations from the initial configurations with $p^D_i = 0.05$ and 0.1. (c) Plot of p^C_f and P^C_{LC} against n_d. The red dashed line represents $P^C_{LC} = 0.1$. (d) Plot of $n_d(P^C_{LC} = 0.1)$ against L. The red curve denotes the relation $n_d(P^C_{LC} = 0.1, L) = n_d(\infty) + 1.8 \times L^{-1.15}$, where $n_d(\infty) = 0.0037$. (e) Growths of C clusters from five diamond-type clusters. Growths stop when a stable D cluster appears between every pair of growing C clusters. t means the Monte Carlo time.

$n_d(\infty) = 0.0037(1)$ as in Fig. 8(d). For $n_d = 0.0037$, $p^C_f \simeq 0.75$, which is also very close to $p^C_{\mathrm{crit}f}$ obtained from FSS analyses of the transition for $p^C_i < 0.5$ in Fig. 7. Thus, as n_d increases, the infinite C cluster disappears and the infinite D cluster appears around $n_d = 0.0037$. When there are many growing C clusters from multiseed C clusters, any C cluster stops growing when there occurs a stable D cluster between every pair of growing C clusters, as shown in Fig. 8(e). The number of such stable D clusters increases as n_d increases. For large enough n_d, these D clusters eventually merge with one another to form an infinite D cluster. This mechanism should explain the anomalous percolation transition for $p^D_i > 0.5$ ($p^C_i < 0.5$).

The fourth regime occurs for $4/3 < b < 3/2$, as shown in Fig. 9. As shown in Fig. 9(a), P^C_{LC} exhibits very complicated behavior. To understand the rapid decrease of P^C_{LC} for $p^C_i < 0.5$, the maximal value $P^C_{\mathrm{max}LC}$ of $P^C_{LC}(L)$ for $p^C_i < 0.5$ is analyzed to find $P^C_{\mathrm{max}LC}(L) = P^C_{\mathrm{max}LC}(\infty) - 5.2(2) \times L^{-0.6(1)}$ with $P^C_{\mathrm{max}LC}(\infty) = 0.76(1)$ [Fig. 9(b)]. Furthermore, $p^C_i(P^C_{\mathrm{max}LC}) \sim L^{-0.48(1)}$ [Fig. 9(c)]. Hence, in the limit $L \to \infty$ there should exist a singular behavior, $P^C_{LC} = 0.76(1)$ at $p^C_i \to 0$ and $P^C_{LC} = 0$ for $p^C_i > 0$. P^C_{LC} for $p^C_i > 0.8$ or large p^C_i in the fourth regime shows nearly the same percolation transition as that in the third regime. From the same FSS analyses for $p^C_i > 0.8$, the same critical exponents

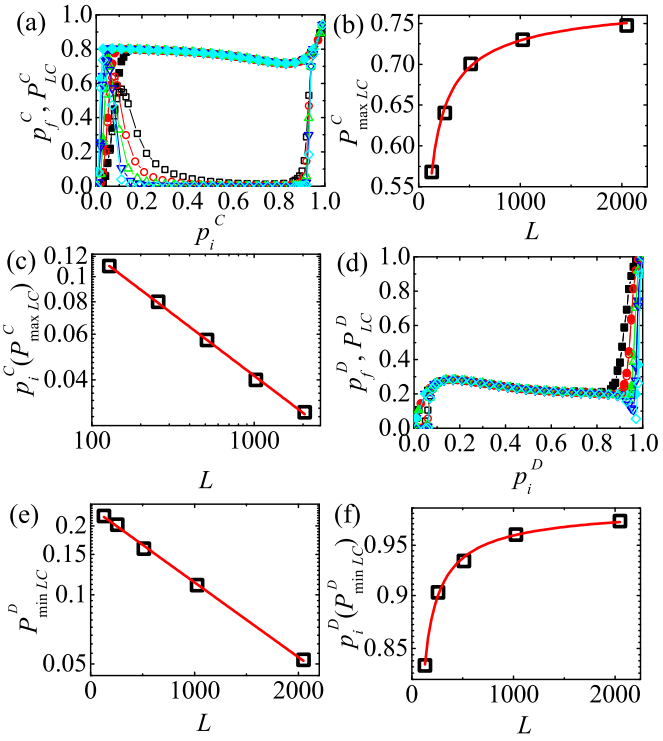

FIG. 9. (Color online) Plots of the fourth regime or for $4/3 < b < 3/2$. (a) Plots of $p_f^C(p_i^C,L)$ and $P_{LC}^C(p_i^C,L)$ against p_i^C. (b) Plot of $P_{\max LC}^C$ against L. The red curve represents the relation $P_{\max LC}^C(L) = P_{\max LC}^C(\infty) - 5.2 \times L^{-0.6}$ with $P_{\max LC}^C(\infty) = 0.76$. (c) Plot of $p_i^C(P_{\max LC}^C)$ against L. The straight line represents the relation $p_i^C(P_{\max LC}^C) = 1.10 \times L^{-0.48}$. (d) Plots of $p_f^D(p_i^D,L)$ and $P_{LC}^D(p_i^D,L)$ against p_i^D. (e) Plot of $P_{\min LC}^D$ against L. The straight line represents the relation $P_{\min LC}^D = 0.245 \times \exp(-0.0007L)$. (f) Plot of $p_i^D(P_{\min LC}^D)$ against L. The red curve represents the relation $p_i^D[P_{\min LC}^D(L)] = p_i^D[P_{\min LC}^D(\infty)] - 6.0 \times L^{-1.3}$ with $p_i^D[P_{\min LC}^D(\infty)] = 1.00$.

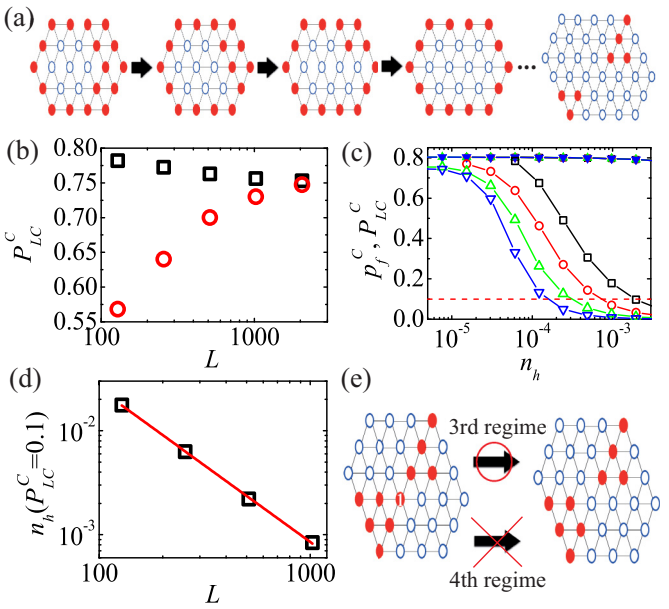

FIG. 10. (Color online) (a) Evolution of an initial configuration of a hexagonal-type C cluster in the fourth regime. (b) Plots of P_{LC}^C from the initial configuration with a single hexagonal-type C cluster (the black square symbols) and $P_{\max LC}^C$ (the red circle symbols) against L. (c) Plots of p_f^C and P_{LC}^C against the density of a hexagonal-type seed C cluster (n_h). The red dashed line represents $P_{LC}^C = 0.1$. (d) Plot of $n_h(P_{LC}^C = 0.1)$ against L. The red line represents $n_h(P_{LC}^C = 0.1) = 22 \times L^{-1.47}$. (e) An example of hindering effects against the merging of two growing C clusters in the fourth regime. If the selected site is the ① D site, the selected D site changes into the C site because the highest payoff of NN C sites is 4 and that of NN D sites is $3b$. In the third regime, $3b < 4$ and the selected site changes into the C site. However, in the fourth regime, the D site does not change its strategy because $3b > 4$.

as those of the random percolation and $p_{crit\,f}^C = 0.7665(1)$ are obtained. P_{LC}^D also exhibits very complicated behavior, as shown in Fig. 9(d). The minimal value $P_{\min LC}^D$ of P_{LC}^D for $p_i^D > 0.5$ satisfies the relation $P_{\min LC}^D \sim \exp(-aL)$ with $a = 0.0007(1)$ and $p_i^D[P_{\min LC}^D(L)] = p_i^D[P_{\min LC}^D(\infty)] - 6.0(5) \times L^{-1.3(1)}$ with $p_i^D[P_{\min LC}^D(\infty)] = 1.00(1)$ [Figs. 9(e) and 9(f)]. The results in Figs. 9(e) and 9(f) confirm the singular behavior, $P_{LC}^D = 0$ at $p_i^D \to 1$ and $P_{LC}^D \simeq 0.2$ in the vicinity of $p_i^D \simeq 1$, corresponding to $P_{LC}^C = 0.76(1)$ at $p_i^C \to 0$. P_{LC}^D for $p_i^D < 0.2$ shows the percolation transition, which corresponds to the percolation transition of C clusters for $p_i^C > 0.8$. From the same FSS analyses, the universality of this D cluster transition is confirmed to belong to that of the random percolation, and $p_{crit\,f}^D = 0.2335(1) (= 1 - p_{crit\,f}^C)$ is obtained.

The growth mechanism of the D cluster in the fourth regime is the same as that in the third regime. Thus, any steady state is an absorbing state [3]. The percolation transition for $p_i^D < 0.2$ ($p_i^C > 0.8$) comes from nearly the same origin as that for the same transition in the third regime. To understand the singular behavior at $p_i^C \to 0$ ($p_i^D \to 1$), the growth mechanisms of both C clusters and D clusters must be considered. In the fourth regime, the hexagonal-type C cluster is not only stable but grows into a large C cluster in which the hexagonal-type C clusters overlap and connect to one another, as shown in Fig. 10(a). As shown in Fig. 10(b), P_{LC}^C of the grown cluster from a single hexagonal-type seed C cluster approaches 0.76 in the limit $L \to \infty$. Therefore, the growing C cluster from a single hexagonal-type seed C cluster is the origin of the singular behavior $P_{LC}^C = 0.76(1)$ at $p_i^C \to 0$. To understand this singular behavior, the dependences of p_f^C and P_{LC}^C on the density n_h of the hexagonal-type seed C clusters are investigated as in Fig. 10(c). Since $n_h(P_{LC}^C = 0.1) \sim L^{-1.47(1)}$ [Fig. 10(d)], the behavior $P_{LC}^C = 0$ for $p_i^C > 0$ in the limit $L \to \infty$ should originate from multigrowing C clusters. The behavior of P_{LC}^C for $p_i^C > 0$ can be explained in the following way. In the case of Fig. 10(e), we clearly see the difference between a merging process of growing C clusters in the third regime and that in the fourth regime. When two growing C clusters are separated by a D cluster as in Fig. 10(e), the ① D site is stable in the fourth regime, while it is unstable in the third regime, as explained in the caption of Fig. 10(e). Thus, the two C clusters merge into a larger cluster in the third regime, but the two clusters cannot merge in the fourth regime. In the limit $L \to \infty$, such hindering effects of D clusters against merges of C clusters get more enhanced and prevent growing C clusters from merging into an infinite C cluster. Only a growing C cluster from a single seed C cluster evolves into an infinite C

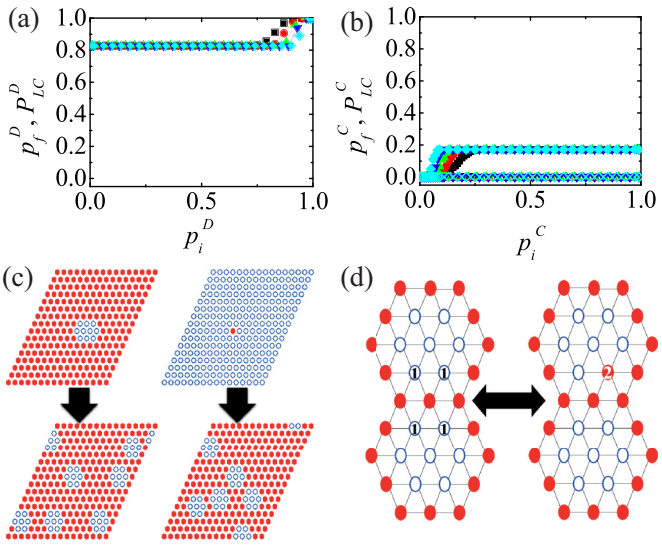

FIG. 11. (Color online) Plots of the fifth regime or for $3/2 < b < 5/3$. (a) Plots of $p_f^D(p_i^D, L)$ and $P_{LC}^D(p_i^D, L)$ against p_i^D. (b) Plots of $p_f^C(p_i^C, L)$ and $P_{LC}^C(p_i^C, L)$ against p_i^C. (c) Steady-state configuration from the initial configuration with an overlapping hexagonal-type C cluster and that from the initial configuration with an isolated D site in the fifth regime. (d) The local strategy reversal process: If the selected site is one of the ① sites, the strategy of the site changes into D because $4b > 6$. However, the strategy of a site such as ② immediately changes back to C because $5 > 3b$.

cluster. This growing mechanism in the fourth regime causes the singular behavior of P_{LC}^C and P_{LC}^D at $p_i^C \to 0$ (at $p_i^D \to 1$).

The fifth regime in which $p_f^C \simeq 0.17$, $P_{LC}^C \simeq 0$, and $P_{LC}^D \simeq p_f^D \simeq 0.83$ [Figs. 11(a) and 11(b)] occurs for $3/2 < b < 5/3$. In the fifth regime, the D cluster always percolates and only finite C clusters exist in the steady state. In this regime, the hexagonal-type C cluster cannot grow but is stable. Instead, any C cluster of overlapping-hexagonal-type evolves to produce scattered hexagonal-type C clusters as in the top left panel of Fig. 11(c). The local strategy reversal process occurs as in Fig. 11(d), in which two hexagonal-type C clusters face each other. But such configurations occur very rarely in the steady state. On the other hand, the triangular ends of D clusters as in Fig. 8(a) (1–4) as well as the free end of the line-part can grow into an infinite cluster. Therefore, the evolution from any initial configuration stops if there remain only isolated hexagonal-type C clusters in the sea of D sites, as in Fig. 11(c).

The sixth regime in which $p_f^C \simeq 0$ and $p_f^D \simeq 1$ occurs for $5/3 < b < 2$, as shown in Figs. 12(a) and 12(b). The D cluster always percolates and only very small finite C clusters exist in the steady state. The small finite C clusters are hexagonal-type or overlapping hexagonal-type C clusters. The hexagonal-type C clusters are stable. In contrast, local strategy reversal processes occur at the edges of the overlapping hexagonal-type C clusters, as shown in Fig. 12(c). However, these reversal processes do not affect the percolation behavior. On the other hand, the growth mechanism of the D cluster is nearly the same as that in the fifth regime. Hence, in the steady state an infinite D cluster and only very small C clusters remain in the steady state.

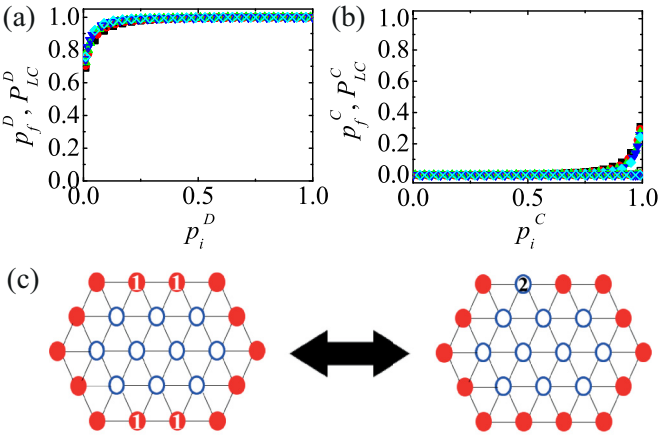

FIG. 12. (Color online) (a) Plots of $p_f^D(p_i^D, L)$ and $P_{LC}^D(p_i^D, L)$ against p_i^D in the sixth regime or for $5/3 < b < 2$. (b) Plots of $p_f^C(p_i^C, L)$ and $P_{LC}^C(p_i^C, L)$ against p_i^C. (c) An example of a local strategy reversal process in this regime. If the selected site is one of the ① sites, the strategy of the site changes into C because $4 > 2b$. However, the strategy of a site such as ② immediately changes back to D because $3b > 5$.

C. Hexagonal lattice

In this section, we explain two regimes occurring on the hexagonal lattice.

The first regime occurs for $1 < b < 3/2$, as shown in Fig. 13. In this regime, p_f^C monotonically increases with p_i^C, as shown in Fig. 13(a). The percolation transition of C clusters is clearly observed, because $P_{LC}^C \simeq 0$ for $p_i^C < 0.7$ and $P_{LC}^C > 0$ for $p_i^C > 0.7$. Using the same FSS analyses, we obtain $1/\nu = 0.75(1)$, $\gamma/\nu = 1.78(1)$, $\beta/\nu = 0.11(1)$, and $p_{\mathrm{crit}f}^C = 0.6326(1)$, which shows that the universality of the transition also belongs to that of the random percolation. p_f^D also monotonically increases with p_i^D. The percolation transition of D clusters is also observed, because $P_{LC}^D \simeq 0$ for $p_i^D < 0.4$ and $P_{LC}^D > 0$ for $p_i^D > 0.4$ [Fig. 13(b)]. Using the FSS analyses, we obtain the same critical exponents as those of the C-cluster transition and $p_{\mathrm{crit}f}^D = 0.6085(1)$. Hence, both C clusters and D clusters undergo percolation transitions with the universality class of the random percolation in the first regime.

In the first regime, the Y-type C cluster and overlaps of Y-type C clusters in Fig. 14(a) are stable. On the other hand,

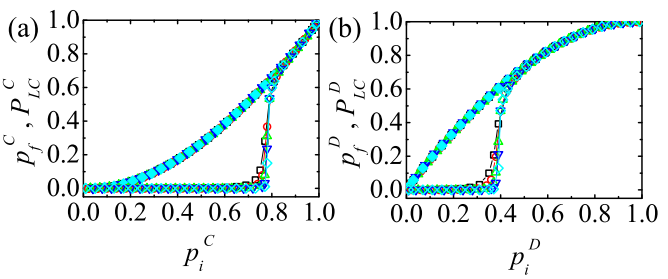

FIG. 13. (Color online) Plots of the first regime or for $1 < b < 3/2$ on the hexagonal lattice. (a) Plots of $p_f^C(p_i^C, L)$ and $P_{LC}^C(p_i^C, L)$ against p_i^C. (b) Plots of $p_f^D(p_i^D, L)$ and $P_{LC}^D(p_i^D, L)$ against p_i^D.

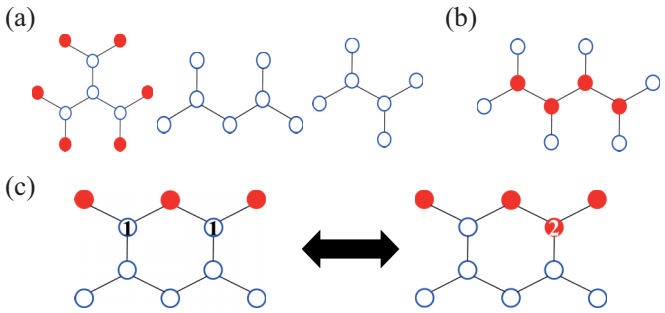

FIG. 14. (Color online) Stable base patterns of (a) C clusters and (b) D clusters in the first regime. (c) An example of a local strategy reversal process in the second regime. If the selected site is one of the ① sites, the strategy changes into D because $2b > 3$. However, the strategy of a site such as ② immediately changes back to C because $2 > b$.

the line-type D clusters with four or fewer sites are stable [Fig. 14(b)]. But any C cluster and D cluster cannot grow into an infinite cluster. Because both C and D clusters exist only in combinations of stable patterns, any steady state is an absorbing state [3]. Thus, in this regime, the connection of such stable clusters is the main mechanism for the percolation transitions.

The second regime occurs for $3/2 < b < 2$. p_f^C monotonically increases from 0 to 0.3 as p_i^C increases from 0 to 1. However, $P_{LC}^C(p_i^C, L) \simeq 0$. Thus, C sites in the steady state form only finite or nonpercolating clusters. In contrast, the infinite D cluster always exists in the steady state, because $P_{LC}^D(\simeq p_f^D)$ increases from 0.7 to 1 as p_i^D increases from 0 to 1. In this regime, any free end of the line-type part of a D cluster can grow, but any C cluster cannot grow. There can occur local strategy reversal processes at the edges of the C cluster shown in Fig. 14(c). However, this reversal process does not affect the percolation behavior. Hence, in the second regime, the D cluster always percolates or forms an infinite cluster, whereas there exist only finite C clusters.

D. Square lattice

On the square lattice, we also find three regimes as in Ref. [19]. In both the first regime for $1 < b < 4/3$ and the third regime for $3/2 < b < 2$, D clusters as well as C clusters undergo the percolation transition. In the second regime for $4/3 < b < 3/2$, D clusters are found to always percolate while C clusters form only finite clusters.

The cluster growth mechanisms as in Secs. II B and II C were never explained in Ref. [19]. Therefore, in this section we mainly explain the mechanisms for three regimes, and we show that the universality of the percolation transition in the third regime cannot be that of a sort of invasion percolation, rather it should be that of the random percolation.

The mechanism of the percolation transition of both C and D clusters in the first regime is nearly the same as in the first regime on the hexagonal lattice. Stable C clusters are combinations of the stable patterns in Fig. 15(a). Stable D clusters are special combinations of the stable patterns in Fig. 15(b). Thus, in this regime, the connection of such stable clusters is the mechanism for the percolation transitions of

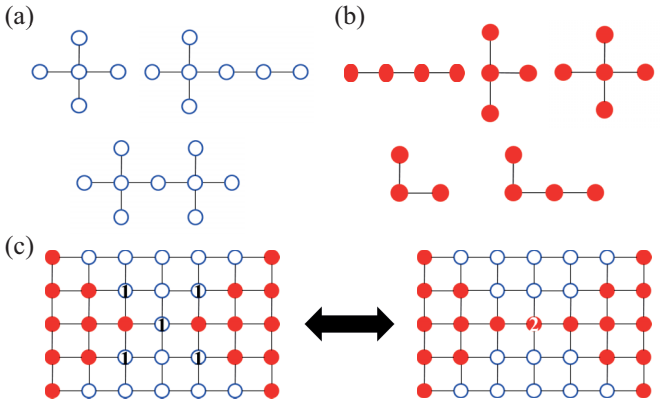

FIG. 15. (Color online) Stable base patterns of (a) C clusters and (b) D clusters in the first regime. (c) An example of a local strategy reversal process in the second regime. If the selected site is one of the ① sites, the strategy changes into D because $3b > 4$. However, the strategy of a site such as ② immediately changes back to C because $3 > 2b$.

both C and D clusters. As in the first regime on the hexagonal lattice, any steady state is also an absorbing state [3] because both C and D clusters consist of stable patterns.

The mechanism in the second regime is nearly the same as that in the second regime on the hexagonal lattice. The free end of the line-type part of a D cluster can grow. Such growth always makes an infinite D cluster. Hence, in the limit $L \to \infty$, $P_{LC}^C \to 0$ although $p_f^C > 0$, whereas $P_{LC}^D \simeq p_f^D > 0$ for all p_i^D. As in the second regime on the hexagonal lattice, local strategy reversal processes occur between the special finite C clusters, as shown in Fig. 15(c). However, these processes do not affect the macroscopic behavior either.

In the third regime, the mechanism is nearly the same as that in the second regime except for the special stable D clusters. When a growing D cluster becomes a compact D cluster in which every D site has at least two D NNs as in Fig. 16, the D cluster cannot grow and become stable. Therefore, for very small $p_i^D (p_i^D < 0.04)$, D clusters in the steady state are only the isolated compact clusters or $P_{LC}^D \simeq 0$ [Fig. 17(a)] and thus the C cluster percolates [Fig. 17(b)]. As p_i^D increases, the number of such stable D clusters increases. For $p_i^D > 0.05$, such compact D clusters merge with one another to form an infinite cluster, i.e., $P_{LC}^D > 0$ [Fig. 17(a)], and there remain only finite C clusters [Fig. 17(b)]. Thus, because many of the D clusters can grow except for the compact D clusters in the third regime, the infinite D cluster appears for much smaller p_i^D in the third regime than in the first regime. As in the first regime on the square lattice, any steady state is an absorbing state [3].

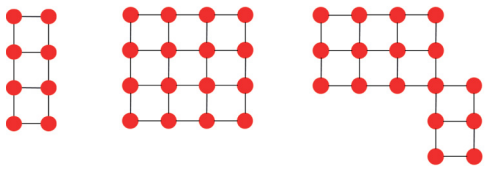

FIG. 16. (Color online) Some stable base patterns of D clusters in the third regime.

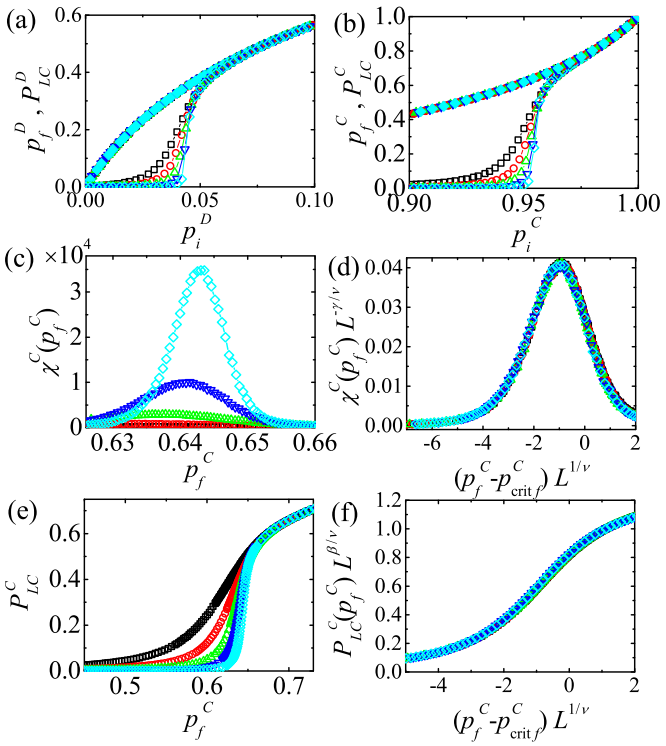

FIG. 17. (Color online) Plots of the third regime or for $3/2 < b < 2$ on the square lattice. (a) Plots of $p_f^D(p_i^D, L)$ and $P_{LC}^D(p_i^D, L)$ against p_i^D for $p_i^D < 0.1$. (b) Plots of $p_f^C(p_i^C, L)$ and $P_{LC}^C(p_i^C, L)$ against p_i^C for $p_i^C > 0.9$ ($p_i^D < 0.1$). (c) Plots of $\chi^C(p_f^C, L)$ against p_f^C. (d) The scaling plot of $\chi^C(p_f^C, L)L^{-\gamma/\nu}$ against $(p_f^C - p_{crit\,f}^C)L^{1/\nu}$ with $p_{crit\,f}^C = 0.6460$, $\gamma/\nu = 1.78$, and $1/\nu = 0.75$. (e) Plots of $P_{LC}^C(p_f^C, L)$ against p_f^C. (f) The scaling plot of $P_{LC}^C(p_f^C, L)L^{\beta/\nu}$ against $(p_f^C - p_{crit\,f}^C)L^{1/\nu}$ with $\beta/\nu = 0.11$.

Because the universality of the percolation transition of C clusters in the third regime was argued to belong to that of invasion percolation with trapping (Ref. [19]), we carefully study the transitions in the third regime from the same FSS analyses. We find $p_{crit\,f}^C = 0.6460(1)$, $p_{crit\,f}^D = 0.3540(1)$, $1/\nu = 0.75(1)$, $\beta/\nu = 0.11(1)$, and $\gamma/\nu = 1.78(1)$ as in Figs. 17(c)–17(f). The measured critical exponents are nearly identical to the exact values of the exponents of the random percolation in two dimensions [23]. This result clearly supports the idea that the universality of the percolation transition of C and D clusters in the third regime belongs to that of the random percolation, not that of invasion percolation with trapping. Physically, one should be careful to establish the universality class numerically when there is no theoretical or analytical foundation. In Ref. [19], the universality of the percolation transition of C clusters in the third regime was argued to belong to that of the invasion percolation with trapping [24] only from a numerical estimation of β/ν and γ/ν by the FSS analyses of the data only for C clusters. However, invasion percolation is a special self-organized process for cluster growth. Furthermore, invasion percolation does not have the phase transition, and thus the critical exponents β, ν, and γ cannot be defined. Therefore, in Ref. [19], β/ν of the invasion percolation is estimated by a brute force application of the formula $d_f = d - \beta/\nu$ [23] and from the numerical data for d_f for the invasion percolation [24]. Hence, the estimation in Ref. [19] has no physical and theoretical foundation at all. As can be seen from the cluster formation mechanism in the third regime, there cannot be any special correlation between each pair of compact D clusters because each compact D cluster comes from the growth of a small D cluster. Initially, such small D clusters should be randomly distributed on the lattice. Thus the percolation in the third regime must not be an invasion percolation, rather it must be a random percolation.

III. SUMMARY AND DISCUSSIONS

To understand how cooperation among selfish individuals emerges and persists, we study the large-scale connectivity of C clusters and D clusters in SEPDG on various two-dimensional lattices using the updates of imitation max. From the numerical analyses of the dependences of $P_{LC}^{C(D)}$ and $p_f^{C(D)}$ on $p_i^{C(D)}$, we find that there are six different regimes on the triangular lattice ($z = 6$). In the first and second regimes ($1 < b < 5/4$), the C cluster always percolates while D clusters remain finite. In the third and fourth regimes ($5/4 < b < 3/2$), both C clusters and D clusters undergo percolation transitions. In the fifth and sixth regimes, the D cluster always percolates while C clusters remain finite ($3/2 < b < 5/3$) or cooperators disappear ($5/3 < b < 2$). On the hexagonal lattice ($z = 3$), we find that there are two distinctive regimes. In the first regime ($1 < b < 3/2$), both C clusters and D clusters undergo percolation transitions. For $3/2 < b < 2$, the D cluster always percolates while C clusters form only finite clusters. Finally, on the square lattice ($z = 4$) we find three different regimes as in Ref. [19]. In the first and third regimes ($1 < b < 4/3$ and $3/2 < b < 2$), both D clusters and C clusters show percolation transitions. In the second regime ($4/3 < b < 3/2$), the D cluster always percolates but C clusters form only finite clusters. The detailed mechanisms for the growth of C and D clusters in each regime are also shown. In addition, based on the FSS analysis, we obtain $1/\nu \simeq 0.75$, $\gamma/\nu \simeq 1.78$, and $\beta/\nu \simeq 0.11$ for any observed percolation transition in SEPDG on various two-dimensional lattices. These values are identical with those for the random percolation in two dimensions. Hence, the observed percolation transitions on various two-dimensional lattices belong to the universality class of the random percolation.

As emphasized in the Introduction, the competition between b and z of the base lattice is the main factor to decide percolation properties. The greater variety of percolation properties in the steady state occurs on the lattice with the larger z. In particular, we clearly see that the following theoretical perspectives are right: the structure of any percolating C cluster is compact, whereas the main structure of the percolating D cluster is line-type.

ACKNOWLEDGMENTS

This research was supported by the Basic Science Research Program through the National Research Foundation of Korea (NRF) funded by the Ministry of Science, ICT & Future Planning (NRF-2013R1A1A2057791).

[1] R. Axelrod, *The Evolution of Cooperation* (Basic Books, New York, 1984).
[2] M. A. Nowak, *Evolutionary Dynamics: Exploring the Equation of Life* (Harvard University Press, Cambridge, 2006).
[3] G. Szabó and G. Fáth, Phys. Rep. **446**, 97 (2007).
[4] J. Kim, H. Chae, S.-H. Yook, and Y. Kim, Sci. Rep. **5**, 9381 (2015).
[5] J. Tanimoto and H. Sagara, Biosystem **90**, 105 (2007).
[6] Z. Wang, S. Kokubo, M. Jusup, and J. Tanimoto, Phys. Life Rev. **14**, 1 (2015).
[7] J. Tanimoto, Appl. Math. Computat. **263**, 171 (2015).
[8] K. Shigaki, Z. Wang, J. Tanimoto, and E. Fukuda, PLOS One **8**, e76942 (2013).
[9] M. A. Nowak and R. M. May, Nature (London) **359**, 826 (1992).
[10] G. Szabó and C. Töke, Phys. Rev. E **58**, 69 (1998).
[11] C. Hauert and M. Doebeli, Nature (London) **428**, 643 (2004).
[12] J. Gómez-Gardeñes, M. Campillo, L. M. Floria, and Y. Moreno, Phys. Rev. Lett. **98**, 108103 (2007).
[13] Z. Wang, S. Kokubo, J. Tanimoto, E. Fukuda, and K. Shigaki, Phys. Rev. E **88**, 042145 (2013).
[14] J. Tanimoto, Phys. Rev. E **90**, 022105 (2014).
[15] M. A. Nowak and R. M. May, Int. J. Bifurcation Chaos **03**, 35 (1993).
[16] Z. Wang, A. Szolnoki, and M. Perc, Phys. Rev. E **85**, 037101 (2012).
[17] Z. Wang, A. Szolnoki, and M. Perc, Sci. Rep. **2**, 369 (2012).
[18] M. H. Vainstein, C. Brito, and J. J. Arenzon, Phys. Rev. E **90**, 022132 (2014).
[19] H.-X. Yang, Z. Rong, and W.-X. Wang, New J. Phys. **16**, 013010 (2014).
[20] G. Szabó, J. Vukov, and A. Szolnoki, Phys. Rev. E **72**, 047107 (2005).
[21] J. Vukov, G. Szabó, and A. Szolnoki, Phys. Rev. E **73**, 067103 (2006).
[22] S. Wolfram, Rev. Mod. Phys. **55**, 601 (1983).
[23] D. Stauffer and A. Aharony, *Introduction to Percolation Theory*, 2nd ed. (Taylor and Francis, London, 1992).
[24] S. Schwarzer, S. Havlin, and A. Bunde, Phys. Rev. E **59**, 3262 (1999).
[25] V. Privman, *Finite-Size Scaling and Numerical Simulation of Statistical Systems* (World Scientific, Singapore, 1990).